

IMPLEMENTATION AND VERIFICATION OF $k - kL$ TURBULENCE MODEL

Erdem Dikbaş*
TÜBİTAK SAGE
Ankara, Turkey

Özgür Uğraş Baran†
METU
Ankara, Turkey

ABSTRACT

In this study, we present the first results of a new turbulence model implementation in our compressible finite volume CFD solver. The $k - kL$ turbulence model is based on the ideas of Rotta's two-equation model. Various research groups progressively develop the model, and it is maturing rapidly. According to the results presented by others, the $k - kL$ turbulence model provides superior results compared to other two-equation turbulence models. The improved solutions are observed especially in flows with high adverse pressure gradients, the blunt body wakes and jet interactions. We have implemented the $k - kL$ model in our solver and we are testing it rigorously. This paper presents our results on standard turbulence test cases, which are subsonic flat plate and subsonic wall-mounted bump. The results compare well with the reference study that are previously presented and published by model developers. The $k - kL$ model prevents excessive production of turbulence and dissipation; hence it preserves vortices significantly better than the other RANS models. Therefore, the implemented model is also tested with a transonic fin trailing vortex case and considerably better results are achieved compared to the SST turbulence model.

INTRODUCTION

Computational Fluid Dynamics is still a developing area encompassing numerous numerical methods to address different aspects of flow physics. It is already accepted as a standard

*Senior Researcher in Aerodynamics Division, Email: erdem.dikbas@tubitak.gov.tr

†Asst. Prof. in Mechanical Engineering Dept., Email: ugras.baran@metu.edu.tr

design and analysis tool for most engineering flows, despite its currently unresolved shortcomings. Turbulence is one of the essential flow features that conventional CFD methods cannot precisely simulate. The main reason for this is the considerable gap between discretization sizes achievable with today's computer capacity and the scales of turbulence. This shortcoming is frequently bypassed by applying turbulence models to replicate turbulence effects into the mean flow. Most turbulence models are designed to compute virtual eddy viscosity parameter that characterizes the turbulent fluctuations of the flow variables. Two-equation models are successfully applied in this context. They rely on the idea that these effects are constituted by two independent scales, obtained from two independent transport equations, as explained by Launder and Spalding [1983].

The $k - kL$ turbulence model was first developed by Rotta [1951], and since then, there has not been widespread use among the CFD community. This slow adaptation is essentially associated with third-order velocity gradient content [Menter and Egorov, 2010], which is cumbersome to compute in practice for most finite volume schemes. However, the historical importance of $k - kL$ remains. It should be noted that, this model constitutes the roots of major families of two-equation models such as $k - \varepsilon$ and $k - \omega$, which are incorporated in many modern CFD solvers [Rodi, 2006]. The model has been becoming prevalent in the last few years, after the efforts of Menter and Egorov [2010; 2010], and Abdol-Hamid [2013; 2015].

The prominent distinguishing feature of Rotta's model is that it employs the turbulent length scale (L) concept in the turbulence transport equations. According to this model, the kL parameter is driven by the third velocity gradient with the assumption of homogeneous turbulence. On the other hand, Menter and Egorov [2006] suggest that a second-order velocity gradient should drive the turbulent length scale. This approach helps to avoid tedious computation of third derivatives, especially for three-dimensional domains [Menter and Egorov, 2010]. The second-order gradient term appears in the von Karman length scale calculation, through which the two turbulence transport equations are coupled. The revision of the length scale discussion leads to the development of the $k - \sqrt{k}L$ (KSKL) model, where the preference of $\sqrt{k}L$ parameter is based on historical reasons. KSKL model provides estimation of local breakups at unstable regions of the flow. This feature may result in an unsteady RANS analysis to have an LES-like behavior where several turbulent scales co-exist in the computed flow field.

The most recent efforts have been made by Abdol-Hamid, while he adapted the $k - kL$ model into NASA solvers. He and his colleagues presented and verified the k-kL-MEAH2015 model after applying Menter's idea to Rotta's model [Abdol-Hamid et al., 2016]. It is demonstrated that the $k - kL$ model shows similar or better performance than SST after testing on various problems with different flow regimes. Other variations where quadratic constitutive relationship (QCR) and algebraic Reynolds stress models (ARSM) are incorporated lead performance improvements [Abdol-Hamid, 2019].

In the current study, the k-kL-MEAH2015 turbulence model is implemented into our in-house flow solver. We used subsonic flat plate and subsonic wall-mounted hump problems as initial validation cases. Test results are presented in comparison with the results of the model developers.

METHOD

We have implemented the k-kL-MEAH2015 model in our density-based finite volume solver. Our solver applies HLLC method as the inviscid flux scheme [Toro et al., 1994] and implicit time integration. The software is suited with widely used turbulence models, e.g., Spalart-Allmaras model and $k - \omega$ family. Hybrid RANS-LES models are also supported. Software execution is done fully parallel by MPI libraries. It is possible to input the grids with various element topologies in a wide range of formats.

Theory

The formulation generated by Abdol-Hamid [2015] is utilized for the implementation in the current study. The equations and other relations are presented here for completeness. NASA Langley Turbulence Modeling Resource [Rumsey, 2021] is adopted for set of equations. Scalar transport equations of variables k and kL are given as described in k-kL-MEAH2015 in Eqs. 1-2.

$$\frac{\partial(\rho k)}{\partial t} + \frac{\partial(\rho u_j k)}{\partial x_j} = P - C_\mu^{3/4} \rho \frac{k^{5/2}}{(kL)} - 2\mu \frac{k}{d^2} + \frac{\partial}{\partial x_j} \left[(\mu + \sigma_k \mu_t) \frac{\partial k}{\partial x_j} \right] \quad (1)$$

$$\frac{\partial(\rho(kL))}{\partial t} + \frac{\partial(\rho u_j(kL))}{\partial x_j} = C_{\phi 1} \frac{(kL)}{k} P - C_{\phi 2} \rho k^{3/2} - 6\mu \frac{(kL)}{d^2} f_\phi + \frac{\partial}{\partial x_j} \left[(\mu + \sigma_\phi \mu_t) \frac{\partial(kL)}{\partial x_j} \right] \quad (2)$$

Production term, P , is computed for both k and kL equations using relations in Eqs. 3-6. Here, the production term is expressed in terms of pure strain tensor S_{ij} . Formulations using the vorticity tensor for the production term are also applicable and can be included as an option in our solver. The production term is limited by the expression given in Eq. 7.

$$P = \tau_{ij} \frac{\partial u_i}{\partial x_j} \quad (3)$$

$$\tau_{ij} = \mu_t \left(2S_{ij} - \frac{2}{3} \frac{\partial u_k}{\partial x_k} \delta_{ij} \right) - \frac{2}{3} \rho k \delta_{ij} \quad (4)$$

$$S_{ij} = \frac{1}{2} \left(\frac{\partial u_i}{\partial x_j} + \frac{\partial u_j}{\partial x_i} \right) \quad (5)$$

$$\mu_t = C_\mu^{3/4} \rho \frac{(kL)}{k^{1/2}} \quad (6)$$

$$\min \left(P, 20 C_\mu^{3/4} \rho \frac{k^{5/2}}{(kL)} \right) \quad (7)$$

Parameters used in kL -equation are given in Eq. 8. The second-order gradient of the velocity field, U'' , takes place in the calculation of the von Karman length scale, L_{vk} , which appears

in the $C_{\phi 1}$ function. While implementing the turbulence model into the solver, the gradient of the velocity gradient components is constructed throughout all face and cell centers.

$$C_{\phi 1} = \left[\zeta_1 - \zeta_2 \left(\frac{kL}{kL_{vk}} \right)^2 \right]; C_{\phi 2} = \zeta_3; f_{\phi} = \frac{1 + C_{d1}\xi}{1 + \xi^4} \quad (8)$$

$$L_{vk} = \kappa \left| \frac{U'}{U''} \right|; U' = \sqrt{2S_{ij}S_{ij}} \quad (9)$$

$$U'' = \sqrt{\left(\frac{\partial^2 u}{\partial x^2} + \frac{\partial^2 u}{\partial y^2} + \frac{\partial^2 u}{\partial z^2} \right) + \left(\frac{\partial^2 v}{\partial x^2} + \frac{\partial^2 v}{\partial y^2} + \frac{\partial^2 v}{\partial z^2} \right) + \left(\frac{\partial^2 w}{\partial x^2} + \frac{\partial^2 w}{\partial y^2} + \frac{\partial^2 w}{\partial z^2} \right)}$$

Limiters and constants not given in this paper are used identically with those described in the reference. Boundary conditions for turbulence equations are given in Eqs. 10 and 11 for farfield and wall boundaries, respectively.

$$k_{\infty} = 9 \times 10^{-9} a_{\infty}^2; (kL)_{\infty} = 1.5589 \times 10^{-6} \mu_{\infty} a_{\infty} / \rho_{\infty} \quad (10)$$

$$k_{wall} = (kL)_{wall} = 0 \quad (11)$$

Validation test cases

Zero pressure gradient flat plate:

The test case of the zero-pressure gradient flat plate is described in Figure 1. As perceived from the inlet boundary condition definitions, the test case is specified for compressible flow solvers despite the low-speed free stream flow ($M_{\infty} \sim 0.2$). It is one of the common cases of the AIAA 5th Drag Prediction Workshop [Levy et al., 2014]. In order to keep all the numerical validation test conditions the same, a grid provided in the NASA Turbulence Modeling Resource website is used [Rumsey, 2021]. The grid borrowed for the current study is the structured hexahedral grid with 2x545x385 node points on each axis.

Bump-in-channel:

The bump-in-channel test case is described in Figure 2. Similar to the previous case, this test case is specified for compressible flow solvers. The bump located at the middle triggers flow separation, which is essentially accepted as challenging to model with RANS models. Indeed, many examples of RANS models are not proven to provide credible results in case of flow separation. In order to keep all the inputs the same, a grid provided in the NASA Turbulence Modeling Resource website is used [Rumsey, 2021]. The grid borrowed for the current study is a structured hexahedral grid with 2x705x321 nodes on each axis.

RESULTS

Verification of the Implementation

Verification of the new implementation of the $k - kL$ turbulence model is shown on zero pressure gradient flat plate and bump-in-channel test cases. The data set given in the

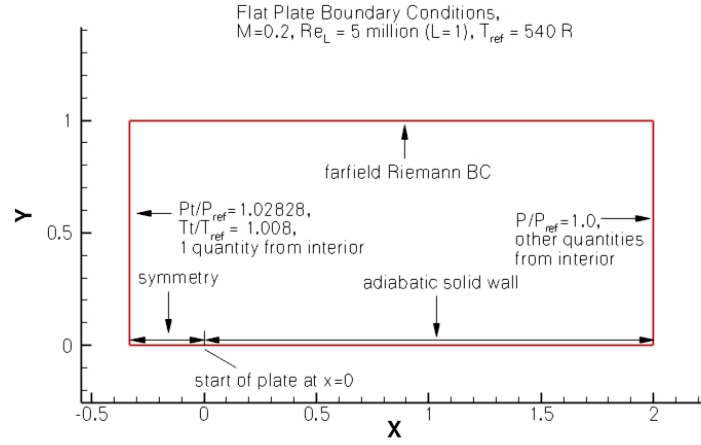


Figure 1: Zero pressure gradient flat plate test case description [Rumsey, 2021]

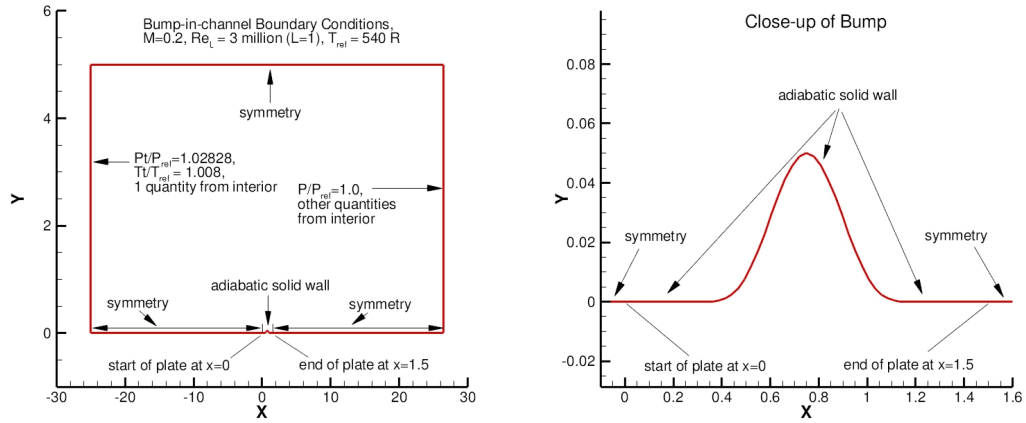


Figure 2: Bump-in-channel test case description [Rumsey, 2021] (not on scale)

NASA Langley Center Turbulence Modeling Resource webpage [Rumsey, 2021] is used for comparison purposes. Local flow field variables at reference planes and variations of flow quantities within the boundary layer at definite axial stations constitute the basis of the comparisons. Results are presented and discussed in the respective sub-headings.

Zero-gradient flat plate:

The zero pressure gradient flat plate case results have been obtained through the utilization of the newly implemented $k - kL$ turbulence model. Verification of current implementation is done via flow field comparison between new results and those presented by Abdol-Hamid [2016]. The computed turbulent viscosity ratio within the boundary layer compares well as given in Figures. 3 and 4. Note that the vertical axes are exaggerated for assessment. The current result of skin-friction coefficient throughout the wall surface mostly coincides with the reference results, except for the foremost region where the gradient of this quantity approaches infinity (Figure 5 – upper left). Velocity, k and kL profiles at $x=0.97$ station also compare very well to the results of the reference study, as seen in Figure 5. Minor differences in the free stream turbulence quantities do not significantly affect the flow field prediction within the boundary layer.

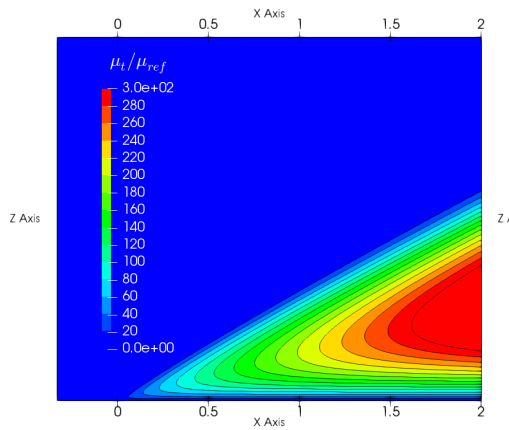


Figure 3: Turbulent viscosity contours within the boundary layer (current); zero-gradient flat plate

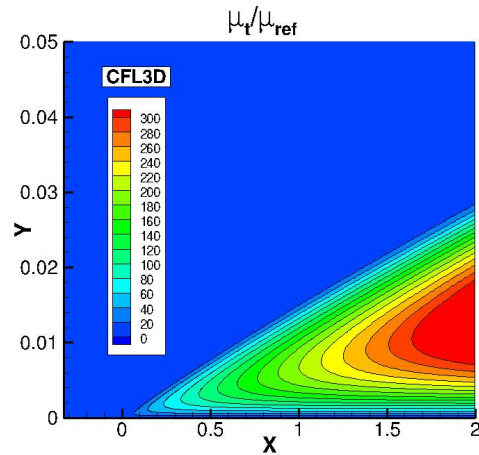


Figure 4: Turbulent viscosity contours within the boundary layer; zero-gradient flat plate (Abdol-Hamid et al. [2016])

Bump-in-channel:

The results of the bump-in-channel case are, at first, examined qualitatively, as in the previous case. Figures 6 and 7 show turbulent viscosity ratio fields computed by current implementation of Abdol-Hamid [2021]. The contour levels are relatively comparable to a particular location near the downstream end of the bump geometry. After this point, slightly higher turbulent viscosity levels are predicted by the current implementation. The difference between maximum values of turbulent viscosity is approximately 10%. This region is exposed to adverse pressure gradient effects; therefore, it is not a surprise to observe deviations here. Although various factors, e.g., flux scheme and wall distance calculation

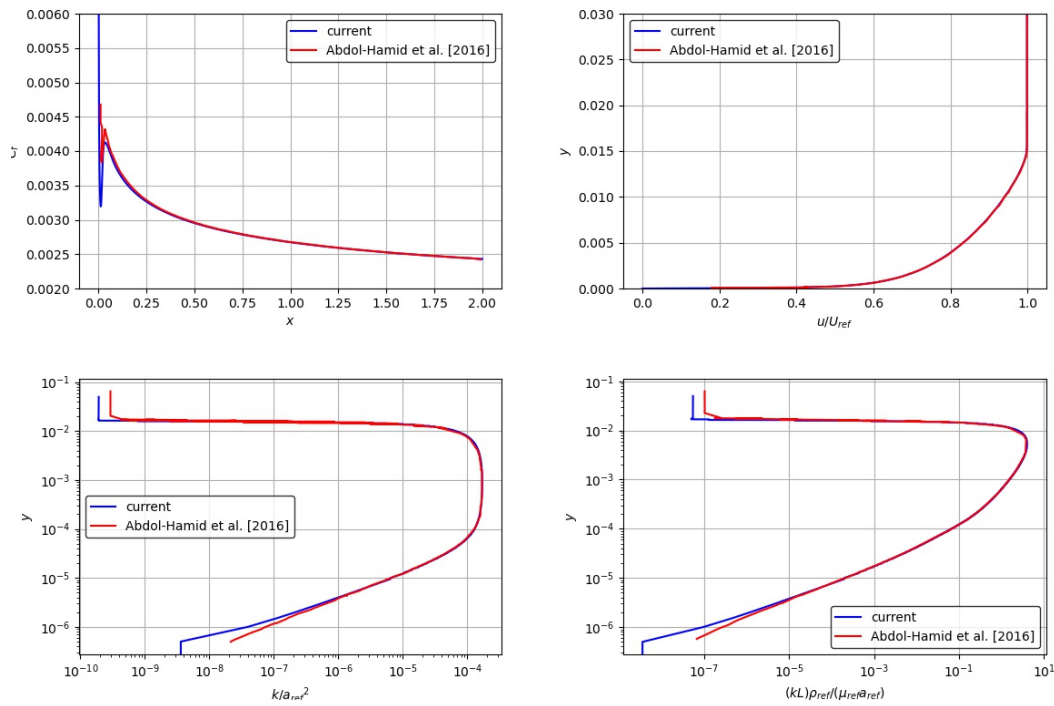


Figure 5: Comparison plots of k-kL results; zero-gradient flat plate case; upper-left: skin friction throughout the plate surface, others: profiles of quantities at $x = 0.97$

method utilized, can be effective, the underlying reason behind this mismatch could not be identified at the moment. The difference in the flow field prediction causes a mismatch in skin friction coefficient for x larger than 0.9, as seen in Figure 8. The same plot also shows that pressure distribution is not affected, and it compares well with Abdol-Hamid's results. Nevertheless, the mismatch is not regarded as an implementation error. The difficulty in predicting adverse pressure gradient region might be why the NASA turbulence modeling website provides the boundary layer profile plots at $x=0.75$ station, i.e. the peak point of the bump geometry. Profile plots in Figure 8 show a good correlation with the reference study and minor differences in free stream turbulence is not effective on boundary layer flow field, similar to the zero pressure gradient flat plate case.

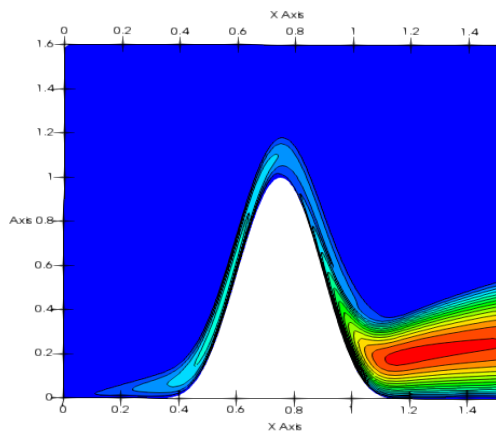


Figure 6: Turbulent viscosity contours within the boundary layer (current); bump-in-channel

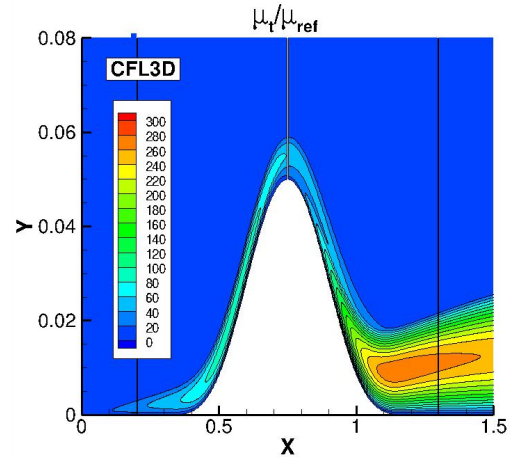


Figure 7: Turbulent viscosity contours within the boundary layer; bump-in-channel (Rumsey [2021])

Fin Trailing Vortex

An experimental study in Sandia National Laboratories investigated the isolated fin aerodynamics in upstream vortex flow generated by another fin [Beresh et al., 2009]. The test was conducted at various speeds in the Mach number range between 0.50 and 0.80. The angles of both fins were adjustable to have different flow conditions. In this study, local flow measurements were conducted without the existence of the aft fin. The outcomes of this effort are considered helpful for the assesment of the current study thanks to the measurements of local flow quantities via particle image velocimetry (PIV) technique. Various parameters such as local velocity vector were measured in cross-planes at different locations providing the velocity deficit and vorticity quantities [Beresh et al., 2012].

Initial observations focused on the fin-tip vortex development in the PIV planes located at four cross-sections downstream the fin at $x/c = 0.51, 1.18, 2.18, 4.18$, with c being root chord length. It was seen that the well-known RANS models could not accurately simulate the vortex core region due to overestimated turbulent viscosity and isotropic turbulence assumption. After $k - kL$ implementation, the fin trailing vortex case is repeated with

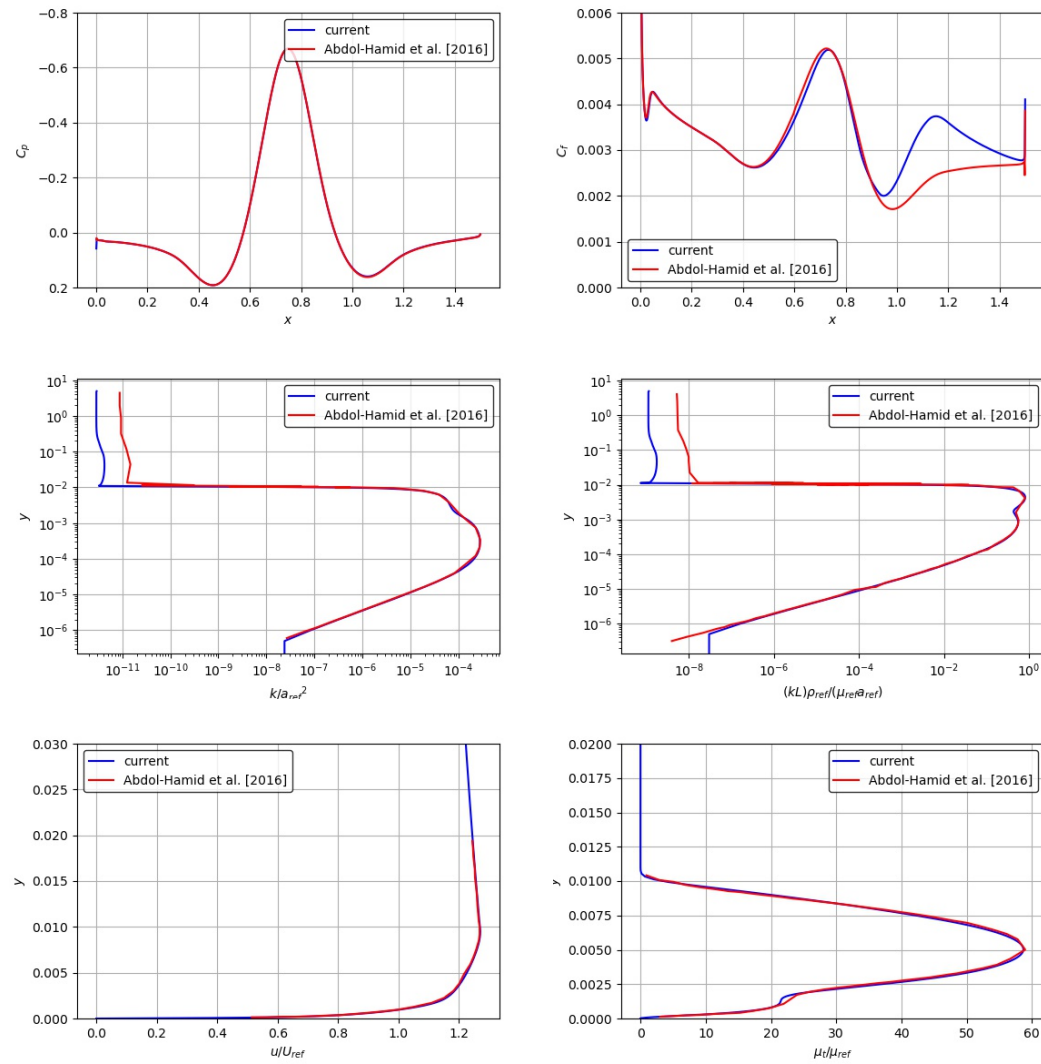


Figure 8: Comparison plots of k-kL results; bump-in-channel; upper-left: skin friction throughout the plate surface, others: profiles of quantities at $x = 0.75$

this turbulence model. The velocity fields showing the vortex core behavior are depicted in Figure 9. It is clear that the vortex is more intensively preserved up to the most downstream cross-plane when $k - kL$ turbulence model is utilized. This behaviour is much closer to the experimental results at the most downstream cross-plane location. We also applied rotation (R) [Dacles-Mariani et al., 1995] and rotation-curvature (RC) [Shur et al., 2000] correction implementations in order to achieve improved results with the SST turbulence model. Tangential velocity profiles through vortex core obtained with all these variants together with those with $k - kL$ are presented in Figure 10. Tangential velocity distribution in the radial direction is much better predicted by $k - kL$ compared to the SST even if any vortex corrections are applied.

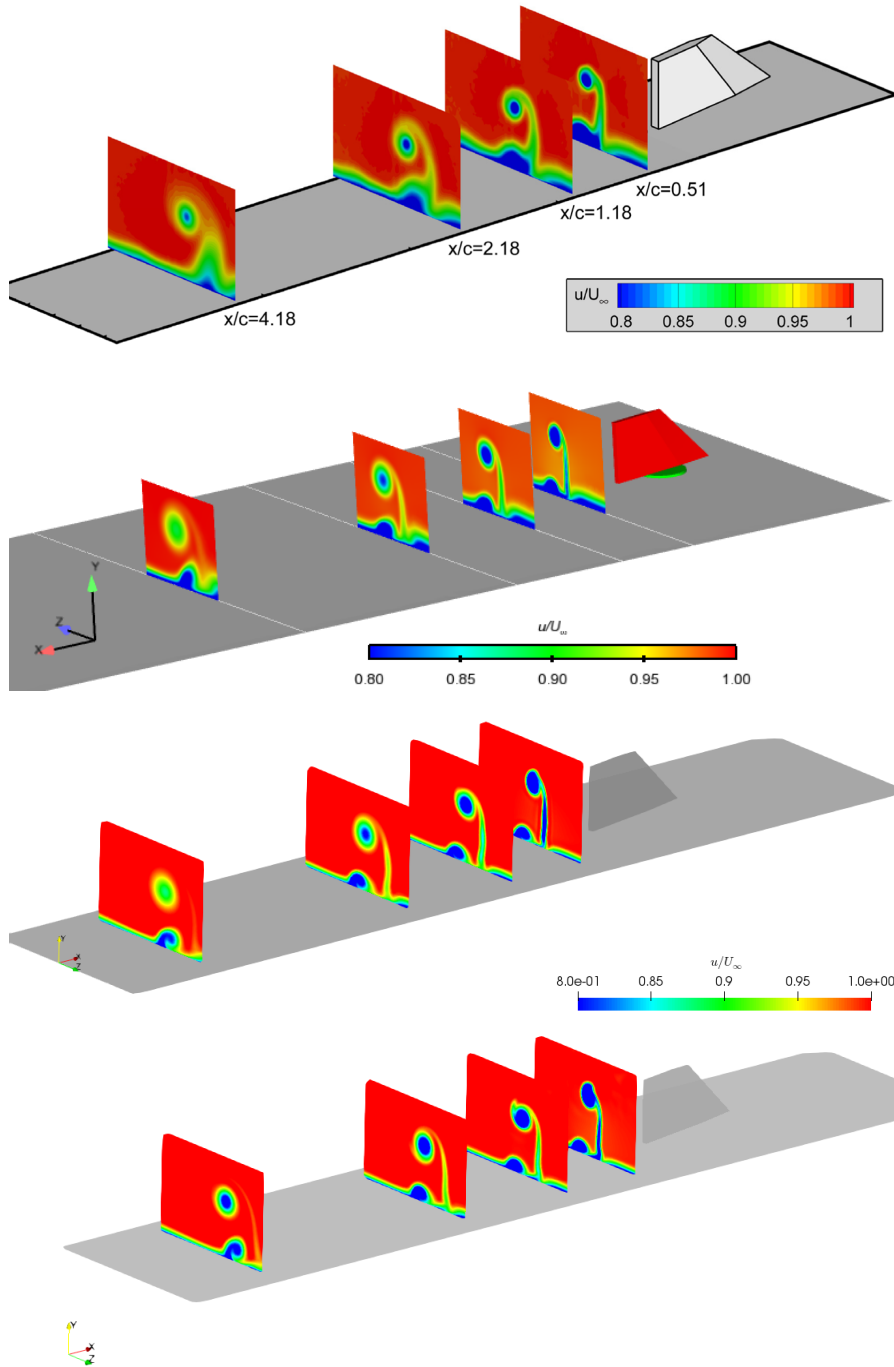


Figure 9: Velocity fields at several cross planes downstream of the fin; top to bottom: i. experiment [Beresh et al., 2009], ii. SST [DeSpirito, 2016], iii. SST (current), iv. $k - kL$ (current); $M_\infty = 0.80$, $Re = 19 \times 10^6 m^{-1}$, $\alpha = 10^\circ$

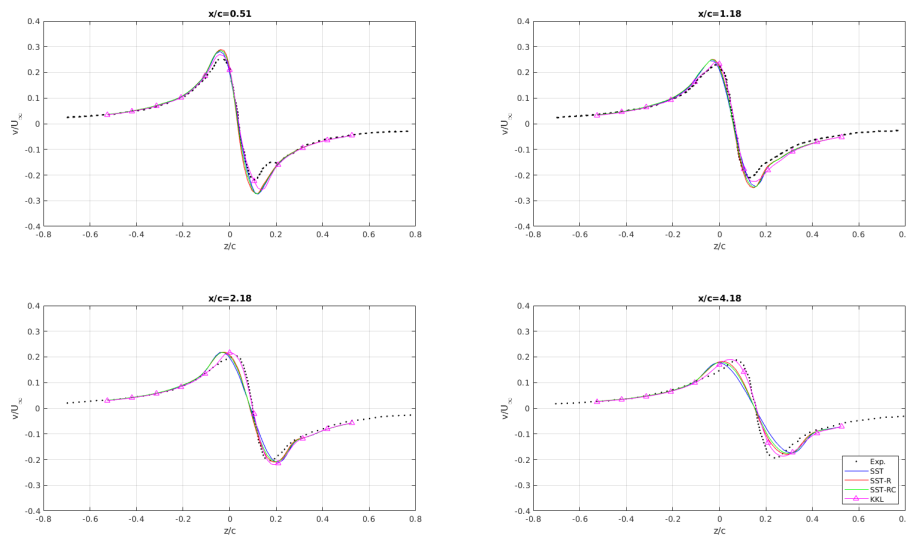


Figure 10: Tangential velocity distribution through vortex core at different cross sections, fin trailing vortex case, experimental results are from Beresh et al. [2009]

CONCLUSION & FUTURE PLAN

In this study, the first results of $k - kL$ turbulence model implementation in our CFD code is presented. Verification work is held using the data generated by the original developers of the model. The results match with adequate margin. The results on the fin trailing vortex case are considerably better than other commonly used two-equation turbulence models. We are currently conducting further validation tests in a broad spectrum. Following studies are going to encompass challenging industrial problems with intensive vortex interactions.

References

- Abdol-Hamid, K. S. (2013). Assessments of-turbulence model based on Menter's modification to Rotta's two-equation model. *International Journal of Aerospace Engineering*, 2015.
- Abdol-Hamid, K. S. (2015). Assessments of k-kL turbulence model based on Menter's modification to Rotta's Two-equation model. *International Journal of Aerospace Engineering*, 2015(March).
- Abdol-Hamid, K. S. (2019). Development of kL-based linear, nonlinear, and full Reynolds stress turbulence models. In *AIAA Scitech 2019 Forum*, page 1878.
- Abdol-Hamid, K. S., Carlson, J.-R., and Rumsey, C. L. (2016). Verification and validation of

- the k-kL turbulence model in FUN3D and CFL3D codes. In *46th AIAA Fluid Dynamics Conference*, page 3941.
- Beresh, S. J., Hen, J. F., and Spillers, R. W. (2009). Planar Velocimetry of a Fin Trailing Vortex in Subsonic Compressible Flow. 47(7).
- Beresh, S. J., Henfling, J. F., and Spillers, R. W. (2012). Turbulence of a fin trailing vortex in subsonic compressible flow. *AIAA Journal*, 50(11):2609–2622.
- Dacles-Mariani, J., Zilliac, G. G., Chow, J. S., and Bradshaw, P. (1995). Numerical/experimental study of a wingtip vortex in the near field. *AIAA Journal*, 33(9):1561–1568.
- DeSpirito, J. (2016). CFD validation of interaction of fin trailing vortex with downstream control surface in high subsonic flow. In *54th AIAA Aerospace Sciences Meeting*, page 1546.
- Egorov, Y., Menter, F., Lechner, R., and Cokljat, D. (2010). The scale-adaptive simulation method for unsteady turbulent flow predictions. part 2: Application to complex flows. *Flow, Turbulence and Combustion*, 85(1):139–165.
- Launder, B. E. and Spalding, D. B. (1983). The numerical computation of turbulent flows. In *Numerical prediction of flow, heat transfer, turbulence and combustion*, pages 96–116. Elsevier.
- Levy, D. W., Laflin, K. R., Tinoco, E. N., Vassberg, J. C., Mani, M., Rider, B., Rumsey, C. L., Wahls, R. A., Morrison, J. H., Brodersen, O. P., et al. (2014). Summary of data from the fifth computational fluid dynamics drag prediction workshop. *Journal of Aircraft*, 51(4):1194–1213.
- Menter, F. R. and Egorov, Y. (2006). Revisiting the turbulent scale equation. In Meier, G. E. A., Sreenivasan, K. R., and Heinemann, H.-J., editors, *IUTAM Symposium on One Hundred Years of Boundary Layer Research*, pages 279–290, Dordrecht. Springer Netherlands.
- Menter, F. R. and Egorov, Y. (2010). The scale-adaptive simulation method for unsteady turbulent flow predictions. Part 1: Theory and model description. *Flow, Turbulence and Combustion*, 85(1):113–138.
- Rodi, W. (2006). Turbulence modelling for boundary-layer calculations. In *IUTAM Symposium on One Hundred Years of Boundary Layer Research*, pages 247–256. Springer.
- Rotta, J. (1951). Statistische theorie nichthomogener turbulenz. *Zeitschrift für Physik*, 129(6):547–572.
- Rumsey, C. L. (2021). Turbulence modeling resource. <https://turbmodels.larc.nasa.gov>. (Accessed on 03/24/2021).

Shur, M. L., Strelets, M. K., Travin, A. K., and Spalart, P. R. (2000). Turbulence modeling in rotating and curved channels: assessing the Spalart-Shur correction. *AIAA journal*, 38(5):784–792.

Toro, E. F., Spruce, M., and Speares, W. (1994). Restoration of the contact surface in the HLL-Riemann solver. *Shock waves*, 4(1):25–34.